GEORG-AUGUST-UNIVERSITÄT
GÖTTINGEN

Superinduktion magnetischer Monopole in spin-ice und Merkmale des thermischen Monopole-noise

Superinduction of magnetic monopoles in spin-ice and monopole noise thermal signature

M.Sc. Abschlussarbeit
im Studiengang theoretische Physik
an der Universität Göttingen

vorgelegt am: 07.04.24

von: H. Zapke, Andrés
1. Gutachter: Prof. P. C. W. Holdsworth[†]
2. Gutachter: Prof. P. Sollich[*]

Universität Göttingen
[†]Laboratoire de Physique, Ecole Normale Supérieure, 46 Alleé d'Italie, Lyon, France
[*]Institute for Theoretical Physics, University of Göttingen, Friedrich-Hund-Platz 1, Göttingen, Germany

Abstract

Modern literature around magnetic monopoles is still consistent with Dirac's picture in that the appearance of a singularity in the vector potential has to be avoided to preserve gauge invariance. The Dirac string represents a valid solution that was confirmed in a single event when an induction experiment measured a current that was consistent with the passage of a monopole and its string. We review the topic, clear up some questions and open up some new. To investigate the analogy with recently discovered quasi-monopole excitations in spin-ice, we introduce slight modifications to the dumbbell model and present a new lattice version of the Helmholtz decomposition, which has proven pivotal to indentify a magnetic coulomb phase. Using quasi-monopoles in spin-ice, we analytically confirm that a magnetic singularity and its string are one inseparable observable to an induction experiment, and that this follows only using the fundamental theorem of vector calculus on the classical electromagnetism of an insulator. We demonstrate this on simulations of a ballistic monopole travelling through a spin crystal, which induces a supercoductive current. Applying this decomposition to the analysis of monopolar power spectra in a thermalized crystal, we provide new insights to preceding studies. A generalized signature of monopolar noise remains inconclusive, different methods for its prediction are proposed.

Contents

1 Motivation

The discovery of magnetic monopole particles would address a number of important questions in modern physics including the origin and composition of dark matter in the universe, the unification of the fundamental forces and the quantization of electric charge. The actual, non-symmetrical form of Maxwell's theory of electromagnetism seems to have withstood the revolution of physics in the 20th century, although not intact. Making considerations of the quantum-mechanical phase change of a wavefunction in an electrical potential, Dirac arrived at his popular quantization condition: $qg = n\hbar c/2$, which, in his own words: *only fixes the product of electric and magnetic charge.* Although in his early consideration of phase changes he finds perfect electromagnetic symmetry[1], he later adds on a Dirac string, connecting magnetic monopole pairs and therefore ensuring $\nabla \cdot \mathbf{B} = 0$[1]. Therefore Dirac monopoles are meant to be used with the classical Maxwell equations and incorporating Dirac strings, to be considered part of his picture.

Having a founder of relativistic quantum mechanics predict magnetic singularities motivated the whole community of experimentalists to search for them. Remarkably, on Valentine's Day of 1982, a researcher at Stanford University [4] was hoping for a monopole to pass through his superconductive coil, and it did. The inducted electrical current was consistent with the passage of one monopole, which had the magnetic charge predicted by Dirac[2]. Sadly this event was only recorded once, therefore closely missing a Nobel Prize. It is to be noted that the expected detection of a dynamic string is not in contradiction with the unobservability of Dirac's (static) strings.

As to this date, the question of magnetic singularities remains open. Research suggests [7]–[9] that these might be found as quasi-particles emerging from condensed matter systems that interact via a Coulomb interaction, as we could confirm with earlier neutron scattering simulations [18]. We used the Helmholtz decomposition [16] of states $\mathbf{M}$ into its fragmented monopolar $\mathbf{M}^m$ and dipolar $\mathbf{M}^d$ parts and studied the scattering of neutrons off the monopolar field-lines that mediate the interaction between this quasi-monopoles. In this study we will show that a Helmholtz decomposition[3] naturally yields a result that includes the Dirac string to the monopolar field $\mathbf{B}_d = \mathbf{B}_{m+string}$. We will compute the induction curves for a ballistic monopole crossing the coil and extend the analysis to the diffusive trajectory of a thermalised monte carlo sample. Computation of the time-correlation function as well as the power spectra will be compared to more recent studies.

1.1 The Stanford experiment reviewed

This experiment drew lots of attention for claiming the detection [4] of a monopole passage through induction (see Figure 1) and it also introduced superconductive coils as the ultimative method for detecting them, due to their direct detection of magnetic flux $I(t) \sim \Phi(t)$, in contrary to common coils $I(t) = \frac{d\Phi}{dt}$ (see section 3.4). We will quickly review their prediction for a current induced by monopole passage.

As stated above, Dirac's theory is meant to be used with the usual Maxwell equations but with a string integrated[4]. The cited reference however starts with the inclusion of monopole current and without a string, which interestingly turns out to be equivalent in our result for the Faraday's induction:

$$\xi = \frac{1}{c}\frac{\partial \Phi}{\partial t} + \vec{j}_m \tag{1}$$

where the left hand side is the *emf* or induced electric potential ξ along the closed coil path Γ, the second term is the change of magnetic flux Φ within the coil and the third is the monopole current, which does not appear in the usual Maxwell equations. If the monopole passes the coil at $t = 0$, we can write $\vec{j}_m = \frac{4\pi}{c} g\delta(t)$. Furthermore, for induction in a superconductor we set $\xi = -L\frac{dI}{dt}$. Plugging in and integrating over time we obtain:

$$-c\,L\,I(t) = \Phi(t) + 4\,\pi\,g\,\theta(t) \tag{2}$$

[1] Maintaining consistency with the classical description $\mathbf{B} = \nabla \times \mathbf{A}$ and with the gauge invariance of $\mathbf{A} \mapsto \mathbf{A} + \nabla\Psi$

[2] Dirac quantiz. with e^-

[3] Also called the fundamental theorem of vector calculus

[4] A Dirac string carries the magnetic flux g away from the sink $(-)$ monopole and into the source $(+)$ monopole, therefore ensuring $\nabla \cdot \vec{B} = 0$ everywhere. This in turn allows the description $\vec{B} = \nabla \times A$

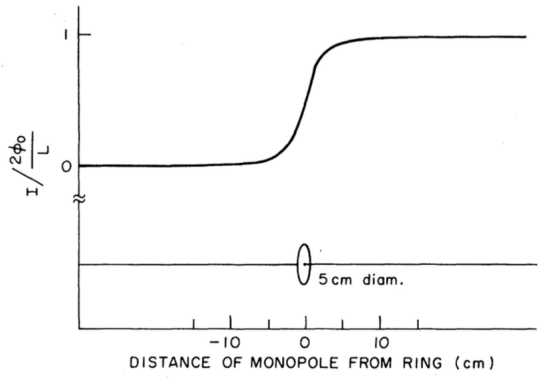

Figure 1: Cabrera's sketch of the induced current due to the passage of a monopole through the SQUID coil

Now for a monopole travelling towards the coil with a velocity v, the author remarkably uses an Ansatz for the flux

$$\Phi = 2\pi g\Big[1 - 2\theta(t) + \frac{\gamma v t}{\big[(\gamma v t)^2 + b^2\big]^{1/2}}\Big] \tag{3}$$

where he subtracts a term $4\pi g\theta(t) = \Phi_{string}$ that can be identified with the flux component of the dirac string[5] (see Figure 2b). Plugging back into eq. 2 this string cancels out with the integrated monopole current $\vec{j}_m$ and we obtain

$$I(t) = -\frac{2\pi g}{cL}\Big[1 + \frac{\gamma v t}{\big[(\gamma v t)^2 + b^2\big]^{1/2}}\Big] \tag{4}$$

yet again the Green curve. We would have obtained the same result when using the induction equation without monopole current but including the Dirac string, therefore the prediction of the Stanford experiment is consistent with Dirac's theory of monopoles. Note that his theory demands the unobservability of the (static) string, which we will prove in the next section. However, the induction setup aims to measure the passing of a dynamic string (dragged by the monopole), therefore this concepts do not stand in contradiction.

Simply put, the dynamic string of a monopole with magnetic charge g travelling along the z-axis:

$$\mathbf{B}_{str}(t) = 4\pi g\,\delta(x)\,\delta(y)\,\Theta(vt - z)\,\mathbf{e}_z \tag{5}$$

will produce a contribution in the coil flux $\Phi_{str}(t) = \int_{S_\Gamma} \mathbf{B}_{str}(t) \cdot d\mathbf{S}$, which can be detected.

1.2 Unobservability and Dirac's quantization. The Aharonov–Bohm effect

As stated in the last section, the Dirac string is considered as a non-observable object, a fact that leads to the Dirac quantization for the product of magnetic and electric charge. However, all derivations of this quantization assume the string to be a classical object, which further motivates the use of quasi-monopoles in spin-ice as a testing ground for its phenomenology. Furthermore, the appearance of the term $\Phi_{str}(t) = \int_S \mathbf{B}_{str}(t) \cdot d\mathbf{S}$ will encourage our lattice formulation of solid-state needles carrying flux Φ in section 2.2.

One of the many derivations of Dirac's quantization is based on the semi-classical interference experiment of a electrically (q) charged particle's wavefunction with a classical, infinite dirac string (Figure 3). The magnetic field is contained within the string, whereas the vector potential $\mathbf{A}$ is defined

[5]We recall that an offset in Φ is irrelevant, since we are not interested in the initial value of the current/flux

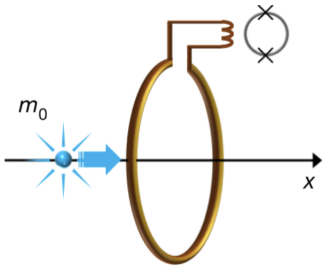

(a) A monopole travelling along z to cross the coil at $t = 0$

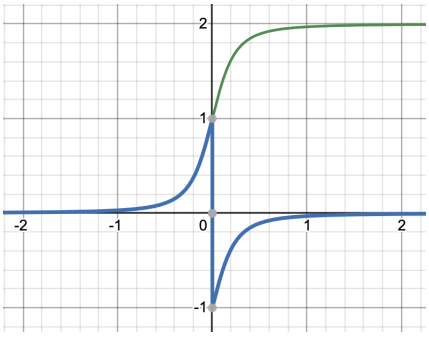

(b) Green: Stanford ansatz for the flux $\Phi = \Phi^{monopole} + \Phi^{string}$. Blue: Only the $\Phi^{monopole}$ contribution

Figure 2: Passage of a monopole through a coil induces a current

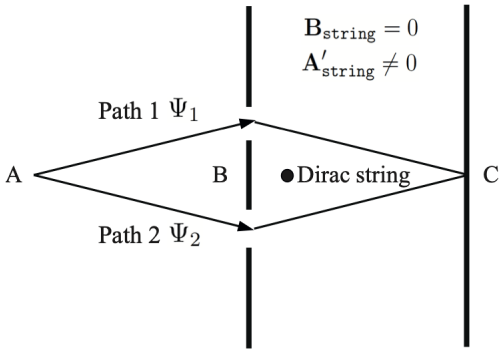

Figure 3: Sketch of a double-slit experiment with an infinite Dirac string $\mathbf{B}_{str}(t) = 4\pi g\delta(x)\delta(y)\mathbf{e}_z$ pointing out of the paper, taken from [13].

everywhere outside the string [6]. We know that $\mathbf{A}$ acts[7] on a wavefunction by shifting the phase of the free particle's solution ψ_0 along the taken path $d\mathbf{l}$:

$$\psi(x,t) = \left(e^{i\frac{q}{\hbar c}\int \mathbf{A}\cdot d\mathbf{l}}\right)\psi_0 \tag{6}$$

This phase change will affect the free solutions of the paths 1 and 2, resulting in interference and ultimately in a resulting amplitude at point C: $P = |\psi_1 + \psi_2|^2$. The sum of wavefunctions yields:

$$\psi = \left(e^{\frac{iq}{\hbar c}\int_1 \mathbf{A}\cdot d\mathbf{l}}\,\psi_1 + e^{\frac{iq}{\hbar c}\int_2 \mathbf{A}\cdot d\mathbf{l}}\,\psi_2\right) \tag{7}$$

Now we realize that the subtraction of both paths gives a closed path ∂S integral around the string, and apply Stoke's theorem, which replaces it with a surface integral S bounded by the closed path. The integrated string's flux gives $4\pi g$ as defined in equation (5).

$$\int_2 \mathbf{A}\cdot d\mathbf{l} - \int_1 \mathbf{A}\cdot d\mathbf{l} = \oint_{\partial S} \mathbf{A}\cdot d\mathbf{l} = \int_S (\vec{\nabla}\times\mathbf{A})\, d\mathbf{S} = \int_S \mathbf{B}_{str}\, d\mathbf{a} = 4\pi g \tag{8}$$

With this insights, we can rewrite equation (7):

[6] We can use $\mathbf{A} = \frac{2g\Theta(r-\epsilon)}{r}\mathbf{e}_\Phi$ in polar coordinates, where ϵ is the width of the string. We will however take a shortcut.

[7] Quantum mechanics, proving that $\mathbf{A}$ is physical and can't have singularities, as required by pure monopoles.

$$\psi = \left(\psi_1 + e^{\frac{iq}{\hbar c}\oint_{\partial S}\mathbf{A}d\mathbf{l}}\,\psi_2\right) e^{\frac{iq}{\hbar c}\int_1 \mathbf{A}\cdot d\mathbf{l}} \tag{9}$$

The global phase will vanish when taking $P = \psi\ \psi^*$. We can impose that the relative phase: $e^{\frac{iq}{\hbar c}4\pi g} = 1$, and we obtain the Dirac quantization:

$$\boxed{qg = n\hbar c/2} \tag{10}$$

If this condition is given, we would obtain the same interference pattern $P = |\psi(t)|^2 = |\psi_1 + \psi_2|^2$ as without a string ($\mathbf{A} = 0$), making the string unobservable to this experiment. Conversely, if the string cannot be detected, it necessarily means that Dirac's quantization is fulfilled. This condition can be used with the known value of the elementary electric charge $q = e^-$ to compute the theoretical value of elementary magnetic charge g_0.

This equation is widely recognized as the reason for electric charge quantization due to its appearance in many different approaches such as the Wu-Yang approach [8] and the 't Hooft–Polyakov monopoles[9]. However, we argue that quantization of the magnetic charge g must be provided alongside Dirac's quantization condition to prove electric quantization, see eq (10). Actually Dirac seemed to be aware of this fact, in his own words: "Our theory thus allows isolated magnetic poles g, but the strength of such poles must be quantised, the quantum g_0 being connected with the electronic charge e^- by $g_0 = \hbar c/(2e^-)$ ... The theory also requires a quantisation of electric charge ....". There seem to be confusion around this fact in all literature since then.

For the interested reader, we explain Dirac's motivation to introduce strings rather than pure monopoles in Appendix A.

1.3 Spin-ice and quasi-monopole excitations

This frustrated magnetic systems have become of major relevance for the research of elusive magnetic monopoles, allowing for experimental access to this particles's consensed-matter analogue but also providing a backbone or medium where they can be simulated [10]. It is commonly described as a crystal of magnetic spin moments m lying on a pyrochlore lattice structure of corner sharing tetrahedra.

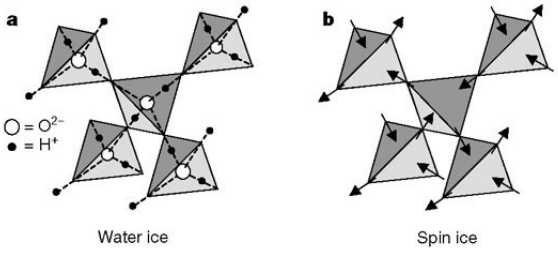

Figure 4: Spin ice and common water ice crystals share the same magnetic moments position geometrically. They are placed between the tetrahedra centers and are forced to point either *in* or *out* of their centers. The nature of the magnetic moment leads however to a different absolute value.

The groundstate is the ensemble of states $\mathbf{M}$ that fulfill the $2in/2out$ rule, which states that each tetrahedron should have 2 spins pointing inward and 2 pointing outward, so as to fullfill the divergenceless condition $\nabla \cdot \mathbf{M} = 0$. An emergent monopole is found in the case that this rule is broken within the neighbours of one tetrahedron. Through one spin flip we can thus create two neighbouring magnetic charges $g_{1,2} = \pm\frac{m}{a}$ where m is the magnetic moment and a is the distance between tetrahedra centers. Subsequent spin flips can generate new monopoles, recombine the existing ones or simply transport the existing ones to other tetratedron.

[8] Which avoids using non-singular potentials, using the single-valuedness of the wave function instead

[9] If the electromagnetic U(1) gauge group is embedded into a non-Abelian gauge group, then charge quantisation is automatic, for considerations of group theory. It is not surprising then that charge quantisation is now considered as an argument in support of grand unified theories

It was shown [7] that the energy difference between two states of the system contains a term for the relative position of the monopoles, which corresponds to a magnetic Coulomb interaction, plus a self energy

$$E = \sum_{i,j} \mu \frac{g_i g_j}{4\pi |\mathbf{r}|} + \sum_i U_i^{self} \tag{11}$$

the latter corresponding to the energy required to generate a monopole (by spin flipping), but also coincidentally equal to the magnetostatic energy stored by the field of the i-th monopole:

$$U_i^{self} = \frac{1}{2} \int |\mathbf{H}_i|^2 d^3\mathbf{r} \tag{12}$$

which gives this conjugate picture the name of *Coulomb phase*. We could therefore leave the moments and instead describe thermally excited magnetic poles subject to generation-recombination process and constrained to the spin-ice lattice.

1.4 Research Problem

We aim to compute the shape of the current induced on a superconductive loop when a quasi-monopole passes in a ballistic trajectory (Fig 5) through it, which has been sketched qualitatively in two papers. We will apply the Helmoltz decomposition and analytically prove that the observable quantity in such an induction experiment is not going to be the total magnetization $\mathbf{M}$ as one would expect. We emphasize on the similarities to a high-energy particle physics experiment [4] which claims to have observed a real monopole passing event and is consistent with our derived observables.

In the second part we will simulate a thermalized sample with diffusive trajectories for the monopoles and compute the induction in frequency space, which can be compared to recent experiments and simulations [15].

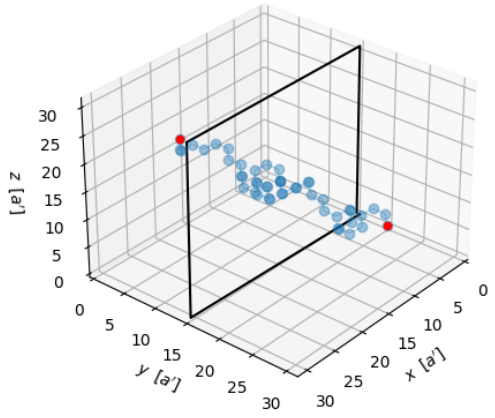

Figure 5: Ballistic trajectory of diamond sites the + monopole will be propagated along.

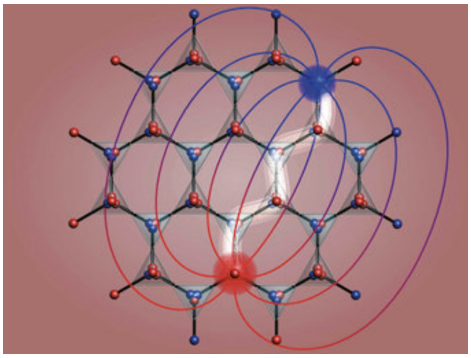

(a) A monopoles pair of the dumbbell model and its resulting, continuous **H** field as envisioned by [7]

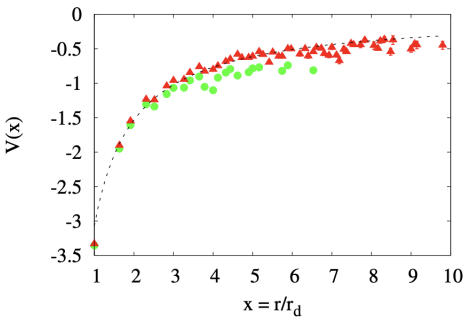

(b) Comparison of energies from the dipolar hamiltonian (markers) to a magnetic coulomb interaction(dashed line)

Figure 6: Magnetic monopoles in dipolar spin-ice

2 Literature Review

2.1 The dipolar picture and the dumbbell picture

The most known model for spin ice includes a nearest neighbour antiferromagnetic term and a dominant, long-range dipolar term (eq. 13) in agreement with neutron scattering experiments [5] we also simulated [18].

$$H = -J \sum_{\langle i,j \rangle} S_i \cdot S_j + Da \sum_{i\langle j} \left[\frac{S_i \cdot S_j}{|r_{ij}|^3} - \frac{3(S_i \cdot r_{ij})(S_j \cdot r_{ij})}{|r_{ij}|^5} \right] \tag{13}$$

A groundbreaking article in 2008 [7] presented an alternative picture, the dumbbell model, replacing localized dipoles by two finitely separated magnetic charges sitting at the tetrahedra centers (Figure 7). Whenever the ground-state symmetry $2in - 2out$ of a tetrahedron was broken, a net magnetic charge Q_I would be present. It was shown that the energy change when flipping dipoles/dumbbells corresponds to a magnetic Coulomb interaction (Figure 6b). Due to the discrete positions of charges I, J the total system's energy V can be written as:

$$V(r_{IJ}) = \begin{cases} \sum_{I \neq J} \frac{\mu Q_I Q_J}{4\pi r_{IJ}} & for \quad I \neq J \\ \frac{1}{2} v_0 Q_I^2 & for \quad I = J \end{cases} \tag{14}$$

Although this model simplifies the energy computation, it is not the most practical description. First, the magnetization $\mathbf{M} = d\mathbf{m}/dV$ is not well defined due to the dipoles of moment $\mathbf{m}$ not being localized [10]. Second, it was claimed that this condensed matter (+) monopoles are a source of H - which lives until now in continuous space, and to fulfill maxwell's equations $\nabla \cdot \mathbf{B} = 0$, a $\mathbf{M}$ (−) sink must appear such that $\nabla \cdot \mathbf{H} = -\nabla \cdot \mathbf{M}$. However the magnetization can't live in empty continuous space and it seems difficult to fulfill divergenceless consistently (see Figure 6a).

In the next section we present a third picture that arises as the next step by extending the dumbbells into a needle of finite cross section dS carrying the same magnetic moment $\mathbf{m}$ and we constraint $\mathbf{H}$ to only be defined within the needle connecting sites I and J. We therefore restrict ourselves to the subspace of the network of needles $\mathbf{r}_{Network} \subset \mathbf{r}$ where $\mathbf{M}$ and $\mathbf{H}$ are well defined on and simplify it to a lattice description $\mathbf{M}_{I,J}$ and $\mathbf{H}_{I,J}$. This will allow us to describe magnetostatics consistently in a lattice, and decompose the lattice fields more easily.

[10] A dipole, which is defined by taking the limit of the distances of the two charges $a \to 0$, can be assigned a moment $\mathbf{m_r}$ at $\mathbf{r}$. Without taking this limit, $\mathbf{r}$ is not defined. In condensed matter physics we rely on being able to assign a position to each moment, as can be seen in equation (1)

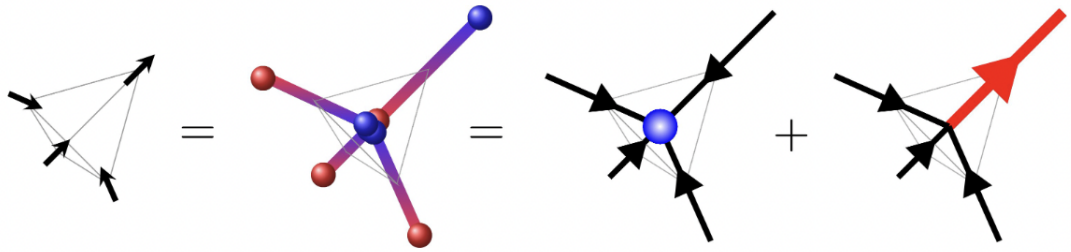

Figure 7: Spin moment picture, dumbbell picture and its fragmented lattice fields M^m_{IJ} and M^d_{IJ}.

2.2 Lattice field theory: the needle model

The dumbbell modell was archieved by replacing infinitesimally short spin-dipoles ($m = g \cdot \tilde{a}$ and $\tilde{a} \to 0$) by two separated charges of $q = \frac{m}{a}$ at its ends [11], therefore conserving the magnetic moment moment m (Figure 7). The consequent step would be to extend the dumbbell's cross section so as to obtain a (material) needle magnet of constant magnetization $\mathbf{M}$, on which we impose $\iiint \mathbf{M} dV = \mathbf{m}$ to conserve $m = |\mathbf{m}|$. Using the known length (NN diamond distance a) we can rewrite it as a integral over the cross-section area [12]

$$\iint \mathbf{M} \cdot d\mathbf{S} = \pm \frac{\mathbf{m}}{a} := \mathbf{M}_{I,J} \tag{15}$$

and denote it $\mathbf{M}_{I,J}$. Dimensional analysis shows that the new defined quantity has coincidentally units of magnetic charge:

$$\mathbf{M}_{I,J} = [\mathbf{M}] \cdot [L^2] = \frac{[\mathbf{m}]}{[L]} = \left[\frac{\mathbf{m}}{a}\right] \tag{16}$$

so $\mathbf{M}_{I,J}$ will take the values ± 1 in units of $[\mathbf{m}/a]$. The charges of the dumbbell model can be recovered by performing the closed surface integral (Gauss's law) of $\mathbf{M}$ at either needle end, as a consequence of the divergent magnetization. Furthermore, we constraint $\mathbf{H}_{I,J} := \int \mathbf{H} \cdot d\mathbf{S}$ to the needles too, so that both quantities are now constrained to the lattice and $\mathbf{B}_{I,J} = \mu(\mathbf{M}_{I,J} + \mathbf{H}_{I,J})$. Note that, although the value $\mathbf{H}_{I,J}$ is not constrained as $\mathbf{M}_{I,J}$, the former is a consequence only of the latter if no external field is applied. Lastly, it can be shown that it also has units of charge, which we then choose to be $\mathbf{H}_{I,J} = \left[\frac{\mathbf{m}}{a}\right]$

In this picture, H-monopoles naturally arise at any junction/diamond site that does not fulfill the divergenceless condition[13] $\nabla \cdot \mathbf{M} \neq 0$. This can be checked by summing over the neighbouring spins in a tetrahedron $Q_I = -\sum_J \mathbf{M}_{IJ}$. For example, Figure 8a represents the configuration $\mathbf{M}$ of one particular ground state in the unit cell. In this case each of the four tetrahedra fulfills the *2in-2out* rule, therefore all I charges give $Q_I = \sum_J \mathbf{M}_{IJ} = -1 - 1 + 1 + 1 = 0$ [10] and there are no monopoles present in the lattice.

[11] $a = a_d \sqrt{2}$ is the NN diamond distance

[12] As Ising spins, only two configurations $\pm\mathbf{m}$ are allowed

[13] Again, the divergences of $\mathbf{M}$ and $\mathbf{H}$ compensate each other to maintain the validity of Maxwell's equations $\nabla \cdot (\mathbf{H} + \mathbf{M}) = 0$.

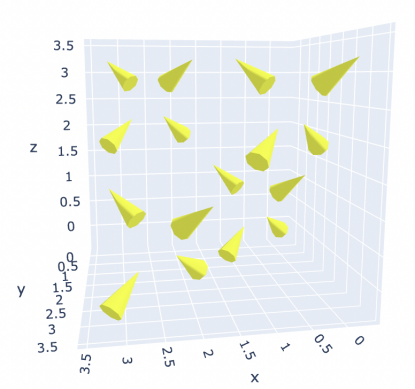

(a) Four tetrahedra, each fulfilling the $2in-2out$ rule. In this particular ground-state, all z-components are positive.

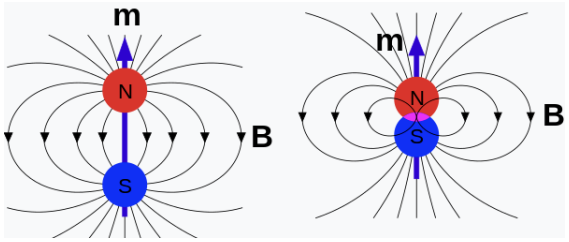

(b) Dipole's $\mathbf{B}$ field in the limit $d \to 0$. In order to maintain $m = q \cdot d$ constant, q has to grow. We argue that the left hand side case delocalizes the moment $\mathbf{m_r}$.

Figure 8: An arrangement of 16 dipoles in a unit cell and the single dipole limit

2.3 Langevin statistics of monopole fluctuations

A thermalised spin-ice sample will experience generation-recombination (GR) and correlated motion of emergent monopoles $\pm g$ interacting via a Coulomb potential but with additional topological constraints given by the underlying spin structure. Recent theories [12] have been developed for the prediction of monopole number N statistics within spin ice. The rates of $\pm g$ pair generation $g(N)$ and recombination $r(N)$ are such that $g(N)|_{N_0} = r(N)|_{N_0}$ where N_0 is the equilibrium number of magnetic charge pairs. Thermally stimulated fluctuations $\delta N = N - N_0$ occur due to this generation and recombination processes. The Langevin equation for these fluctuations has been derived as:

$$\frac{d(\delta N)}{dt} = -\frac{\delta N}{\tau} + \sqrt{A(T)}\eta(t) \tag{17}$$

where the GR rate is $\tau = 1/(dr/dN - dg/dN)|_{N_0}$ and the second term represents the uncorrelated thermal noise. Taking the Fourier transform of eq (17) yields a prediction for the power spectra of monopole number N fluctuations as:

$$S_N(\omega) = \frac{4\sigma_N^2 \tau(T)}{(1 + \omega^2 \tau^2(T))} \tag{18}$$

with $\sigma_N^2 = \langle \delta N^2 \rangle$ being the variance in the number of $\pm g$ pairs. [14]

We are mainly interested in the statistics of the current induced in our coil I_t, which we will later prove to be directly proportional to the magnetic flux passing through the coil $\Phi_t \propto L \cdot I_t$ for superconducting coils. This statistics are best described in terms of the power spectra of the magnetic flux $S_\Phi(\omega)$. In order to bridge the derived power spectra of monopole number $S_N(\omega)$ to our spectra of interest, we will make use of a well-known relation used in intrinsic semiconductors. It was found [6] that in plasmas of $\pm q$ electric charges subject to Coulomb interactions and spontaneous generation/recombination the following relation holds:

$$S_V(\omega) = V^2 \, S_n(\omega)/N_0^2 \propto S_\Phi(\omega) \tag{19}$$

where $S_V(\omega)$ is called voltage noise spectra and we will, for our purposes, identify [15] it with the spectra of induction $S_\Phi(\omega)$.

It is unclear whether this assumption can be simply made, due to the topological constraints of spin-ice being present in monopole $\pm g$ motion but not in the plasma of electric $\pm q$ charges. We will nevertheless make use this approach and explore the possible differences.

[14] This paragraph was adopted from [15].

3 Theoretical Framework

3.1 Helmholtz decomposition (HD)

Starting from a monopole-free configuration $\mathbf{M}^{t=0}$ as in Figure 8a, we can flip one of the needles to create a pair a monopoles in our final configuration $\mathbf{M}^t$. We expect the previous $\mathbf{H}^t$ field from Figure 6a, which is now constrained to the lattice, to resemble Figure 9a, we will derive the decomposition later. We recognise that $\mathbf{H}^t$ remains invariant for any state $\mathbf{M}^t$ that contains monopoles at that same positions. For example any flipping of a closed loop (gauge of the curl) of spins leaves the monopole distribution invariant. This is the reason why gauge theory is a good description of emergence. The decomposed/fragmented fields $\mathbf{M} = \mathbf{M}_d + \mathbf{M}_m$ will reveal many of the interesting emergent properties, with $\mathbf{M}_d$ constituting a fluctuating field of the divergenceless degrees of freedom from whom the magnetic Coulomb phase $\mathbf{H} = -\mathbf{M}_m$ emerges. The latter will recover simply the magnetic field lines of a given charge distribution as when solving Poisson's equations of magnetostatics $\nabla \cdot \mathbf{M}_m = -\rho_m$.

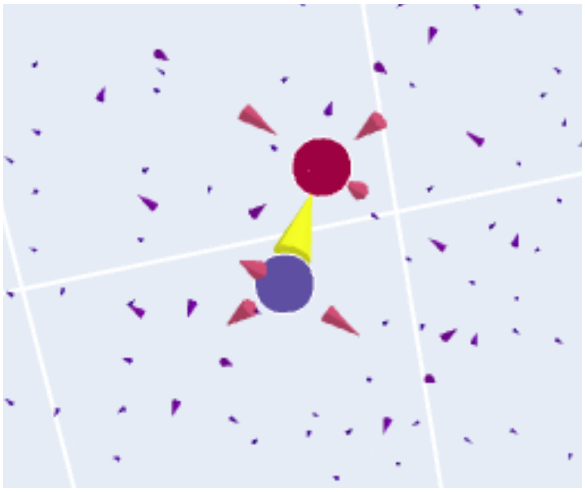

(a) $\mathbf{M}_m$ of a neighbouring monopole pair, obtained from the iterative HHD on the pyrochlore lattice

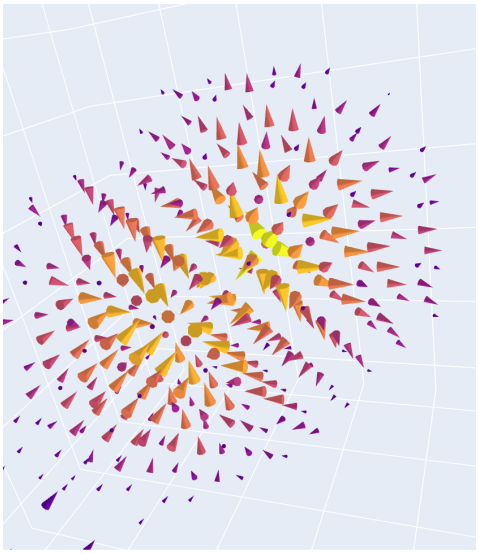

(b) Coarse grained, rescaled version of Figure (a) for a monopole pair at large distances.

Figure 9: The monopolar part $\mathbf{M}_m$ contains the field lines for a given charge distribution

We will present this decomposition as an iterative process that converges monotonically to a divergence-free $\mathbf{M}_d$ and a curl-free $\mathbf{M}_m$ component[15]:

$$\mathbf{M} = \mathbf{M}_m + \mathbf{M}_d = \vec{\nabla}\phi(r) + \vec{\nabla} \times \mathbf{A} \tag{20}$$

This decomposition is unique, as we assume there is no harmonic component present $\Delta\phi_H(\mathbf{r}) = 0$ (external field). In this case, the complementary fields $\mathbf{M}_m + \mathbf{M}_d$ span the whole configuration space $\mathbf{M}$. Furthermore, we know that no electric currents are present (insulator):

$$\nabla \times H = J = 0 \quad \Rightarrow H = H_m \text{ only} \tag{21}$$

And using $\frac{1}{\mu}\mathbf{B} = \mathbf{H} + \mathbf{M}$:

$$\frac{1}{\mu}\nabla \cdot \mathbf{B} = 0 = \nabla \cdot \mathbf{H} + \nabla \cdot \mathbf{M}_m \quad \Rightarrow \mathbf{H} = -\mathbf{M}_m \tag{22}$$

$$\frac{1}{\mu}\mathbf{B} = -\mathbf{M}_m + \mathbf{M}_m + \mathbf{M}_d \quad \Rightarrow \mathbf{B} = \mu \cdot \mathbf{M}_d \tag{23}$$

we obtain the statement made before. We also used that, by definition $\nabla \cdot \mathbf{M}_d = 0$.

[15]Note that the total strength of an element $\mathbf{M}$ is constrained to ± 1 while the fragmented part is not necessarily.

3.2 Iterative, discrete Helmholtz decomposition

The decomposition occurs ultimately in each *spin*: $M_{IJ} = M^m_{IJ} + M^d_{IJ} = \pm 1$. We now introduce the useful four-vector formalism, which describes each site/tetrahedron through its neighbouring spins $M_I = [M_{IJ}, M_{IK}, M_{IL}, M_{IM}]$ with charge $Q_I = \sum_J M_{IJ}$. This algorithm will decompose the four-vectors iteratively and converge to a final solution where the d component is divergenceless everywhere $Q^d_I = \sum_J M^d_{IJ} = 0 \ \forall \ I$ and has been adapted from [16] to the pyrochlore lattice formulation. We choose an example tetrahedron A with initial configuration 3in-1out: $[-1,-1,-1,1]$, thus containing a monopole. Its four neighbour sites fulfill the 2in-2out rule, for example its (first) neighbour B has configuration $[1,1,-1,-1]$, where $M_{AB} = -M_{BA} = -1$ is the common (first) spin. We start with monopolar field $M^0_m = \emptyset$ at iteration zero, therefore our starting configuration is[16]:

$$\begin{aligned} M^0_A &= [-1,-1,-1,1]_d + [0,0,0,0]_m \\ M^0_B &= [1,1,-1,-1]_d + [0,0,0,0]_m \end{aligned} \tag{24}$$

Their initial charges in d are $Q^d_A = -2$ and $Q^d_B = 0$, respectively. We then define the flow of charge between each tetrahedra F_{IJ} as in Equation 25, and calculate the corresponding flux in our example

$$F_{AB} = \frac{Q^d_A - Q^d_B}{8} = -\frac{1}{4} \tag{25}$$

We recall that we would have to compute the fluxes between each pair of tetrahedron F_{IJ} before continuing with the next step. In our example we apply the fluxes between A and B, for the monopolar and dipolar field, defined as:

$$\begin{aligned} A: \ \ M^1_d &= M^0_d - F_{AB} \ \ M^1_m = M^0_m + F_{AB} \\ B: \ \ M^1_d &= M^0_d + F_{AB} \ \ M^1_m = M^0_m - F_{AB} \end{aligned} \tag{26}$$

such that after the first iteration we have:

$$\begin{aligned} M^1_A &= [-\frac{3}{4}, -1, -1, 1]_d + [-\frac{1}{4}, 0, 0, 0]_m \\ M^1_B &= [\frac{3}{4}, 1, -1, -1]_d + [\frac{1}{4}, 0, 0, 0]_m \end{aligned} \tag{27}$$

Now we apply the fluxes between A and the remaining diamond neighbours, which in this example all amount to $F_{AJ} = -1/4$, connected through the remaining spins, to obtain in a first iteration the following configuration in A[17]:

$$M^1_A = [-\frac{3}{4}, -\frac{3}{4}, -\frac{3}{4}, \frac{5}{4}]_d + [-\frac{1}{4}, -\frac{1}{4}, -\frac{1}{4}, -\frac{1}{4}]_m \tag{28}$$

In the second iteration, we again calculate the fluxes F_{IJ} given by the Q^d charges as in equation 25 and apply them on the fields for the corresponding, connecting spin as in 26, iterating until we reach a given condition $Q^d_I < \lambda$ for each site.

In our example we converge to the solution at iteration n:

$$M^n_A = [-\frac{1}{2}, -\frac{1}{2}, -\frac{1}{2}, \frac{3}{2}]_d + [-\frac{1}{2}, -\frac{1}{2}, -\frac{1}{2}, -\frac{1}{2}]_m \tag{29}$$

where the M_d part is divergence-less and the M_m part has a charge of -2 at A because there is a monopole.

[16] We renounce writing down all four neighbours for the sake of clarity

[17] Again, the B-th site itself has four neighbours. Steps from eq. 25 and 26 have to be carried out simultaneously for each site pair I, J before continuing with the second iteration.

While solving for the whole system simultaneously, the monopolar fieldlines are propagated outwards (Figure 9b) and are non-zero even far from the monopoles, creating long-range correlations. In fact they ensure that M^m is also divergenceless everywhere except at the sites containing monopoles.

As a condition for the algorithm we imposed that the divergence of the M_d shall not surpass a certain value anywhere: $Q_d^i < 0.01$, which was met already with few iterations $n \approx 60$ under $20sec$ for a system size of $L = 8$.

3.3 Dirac strings and reference states

Although some static monopoles will be present in our reference sample $\mathbf{M}^0$, we want to focus on the phenomenology of a dynamic monopole travelling the sample. It will be propagated over time t by spin flipping, giving the configuration $\mathbf{M}^t$. Then the $(-)$ change with respect to the reference state $\mathbf{M}_{string} = \mathbf{M}^0 - \mathbf{M}^t$ leaves only the spins of strength $2 \cdot \frac{m}{a}$ connecting the dynamic monopole with its counterpart. This takes the role of a classical Dirac string (Figure 11), at it ensures that $\mathbf{M}_m^t + \mathbf{M}_{dirac}$ is divergence-free. We can prove that using eq. 20 for a initial state without charges $\mathbf{M}_m^0 = 0$:

$$\mathbf{M}_m^t + \mathbf{M}_{dirac} = (\mathbf{M}^t - \mathbf{M}_d^t) + (\mathbf{M}^0 - \mathbf{M}^t) = \tag{30}$$

$$\mathbf{M}^t - \mathbf{M}_d^t + \mathbf{M}_d^0 + \mathbf{M}_m^0 - \mathbf{M}^t = -\mathbf{M}_d^t + \mathbf{M}_d^0 \tag{31}$$

For the case that there is charges in the initial configuration, we define the dynamic monopolar field by subtracting the monopolar reference state $\bar{\mathbf{M}}_m^t = \mathbf{M}_m^t - \mathbf{M}_m^0$ (see Figure 10) and find again:

$$\bar{\mathbf{M}}_m^t + \mathbf{M}_{dirac} = (\mathbf{M}^t - \mathbf{M}_d^t - \mathbf{M}^0 + \mathbf{M}_d^0) + (\mathbf{M}^0 - \mathbf{M}^t) = -\mathbf{M}_d^t + \mathbf{M}_d^0 \tag{32}$$

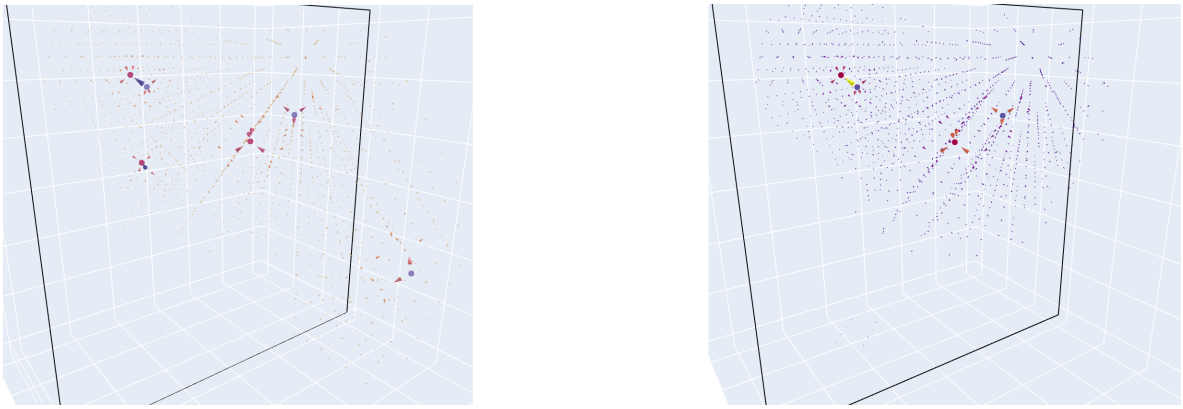

(a) The monopolar field $\mathbf{M}_m^t$ at time t

(b) The reference monopolar field $\mathbf{M}_m^0$

Figure 10: The monopolar part $\mathbf{H} = -\mathbf{M}_m$ contains the field lines for a given charge distribution.

3.4 Induction on a superconductive coil

To find out which field components can be measured by an induction coil we start with Faraday's law for the electromotive force or potential $\xi = -\frac{d\Phi}{dt}$. This will cause a superconductive current $-L\frac{dI}{dt}$ so we can integrate on both sides to obtain:

$$\xi = -\frac{d\Phi}{dt} = -L\frac{dI}{dt} \quad \Longrightarrow \quad (\Phi_t - \Phi_0) = L(I_t - I_0) \implies \Phi_t \sim L \cdot I_t \tag{33}$$

where I_0 and Φ_0 are the reference current and magnetic flux passing the coil, corresponding to the $t = 0$ fields introduced in last section. We already carried integration of the fields over the needle cross sections when we introduced the lattice description $\mathbf{B}_{IJ} = \int \mathbf{B}_{needle} \cdot d\mathbf{S}_{needle}$ [18], so the integral over the coil becomes just the sum of $\mathbf{B}_{IJ}$:

[18] And every field is zero outside of the needle network

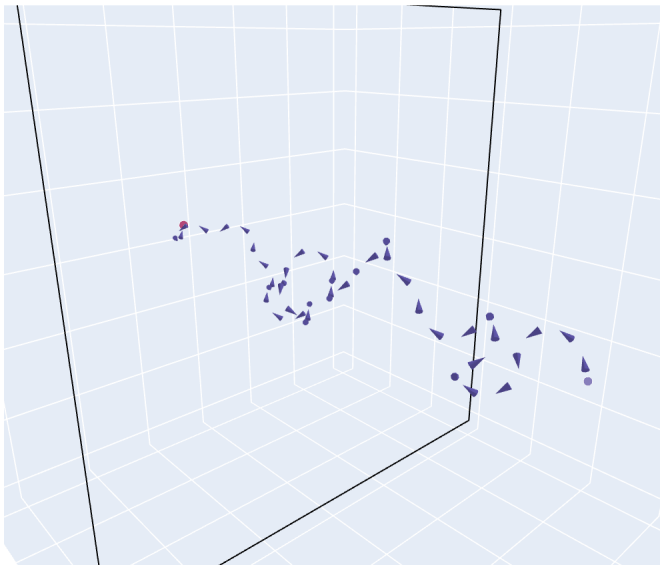

Figure 11: Blue Dirac string: Ballistic trajectory of spins that will be flipped. Red $(-)$ and blue $(+)$ spheres represent monopole pairs and their surrounding monopolar fields. The two upper pairs are static monopoles.

$$\Phi = \int \mathbf{B} \cdot d\mathbf{S} = \sum_{IJ}^{coil} \mathbf{B}_{IJ} = \sum_{IJ}^{coil} \mu \cdot \mathbf{M}_{d,IJ} \tag{34}$$

where we used eq. (23). This in turn means that, using eqs (32) and (22), we obtain the difference

$$\Phi^t - \Phi^0 = \mu \sum_{IJ}^{coil} (\mathbf{M}_d^t - \mathbf{M}_d^0) = -\mu \sum_{IJ}^{coil} (\mathbf{M}_{dirac} + \mathbf{M}_m^t) = \mu \sum_{IJ}^{coil} (-\mathbf{M}_{dirac} + \mathbf{H}) \tag{35}$$

which is divergenceless by definition, but it also has the units of magnetic field through the coil B. We will use the bar to define sums over the coil $\overline{\mathbf{M}}_d = \sum_{IJ}^{coil} \cdot \mathbf{M}_{d,IJ}$ and drop the reference flux:

$$\boxed{\Phi^t \approx \overline{\mathbf{B}}_{m+dirac}^t = -\overline{\mathbf{B}}_d^t + \overline{\mathbf{B}}_d^0} \tag{36}$$

along with the (unphysical) induction components that we can compute separately:

$$\boxed{\overline{\mathbf{B}}_d^t = \mu \sum_{IJ}^{coil} \mathbf{M}_d^t \qquad \overline{\mathbf{B}}_m^t = \mu \sum_{IJ}^{coil} \mathbf{M}_m^t \qquad \overline{\mathbf{B}}_{tot}^t = \mu \textstyle\sum_{IJ}^{coil} \mathbf{M}^t} \tag{37}$$

The Helmholtz theorem yields therefore following statement: We can't measure monopole field and string separately, only as a complete classical system, whose change is negatively proportional to the change of the d component $-\Delta\overline{\mathbf{B}}_d^t$.

The flux curve we obtain quantifies the passing of a quasi-monopole and its string, and will serve as a basis for frequency-dependent noise analysis by means of monte carlo simulation. Before preceding with that, we first present all the results for the ballistic monopole crossing the coil. Note that because the needles transport flux rather than flux density, we do not need to take the angle-dependent dot product $\mathbf{B} \cdot d\mathbf{S}$ as in the case of a continuous magnetic field. We do however choose a sign for each spin, depending on whether they point *in* or *out* of the coil.

3.5 Methods: Induction curves for a ballistic trajectory

The ballistic simulation is simple yet very instructive. We already chose a path[19] of diamond sites $\{Q_I\}$ for the + monopole to propagate (see Figure 5) and the corresponding spins between them $\{S_i = M_{IJ}\}$ that have to be flipped (see Figure 11). We flip the spins sequentially over time along the path, effectively moving the "source" of flux ($\nabla \cdot \mathbf{M} \neq 0$) to the next diamond site and obtaining a set of configurations $\mathbf{M}^t$.

At each step t, we will decompose the total configuration $\mathbf{M}^t$ into its $\mathbf{M}_d^t$ and $\mathbf{M}_m^t$ components. We can also recover the dirac string at any time with $\mathbf{M}_{dirac}^t = \mathbf{M}^t - \mathbf{M}^0$. We are however mostly interested in $\mathbf{M}_m + \mathbf{M}_{dirac}$, which will finally quantify the induction curve expected from the Stanford experiment [4] (see section 1.1).

4 Intermediate result

4.1 Induction curves for a ballistic monopole

In Figures 13, the $\mathbf{M}_m + \mathbf{M}_{dirac}$ component has been depicted at three different timessteps t. The monopolar part has been coarse grained over volumes $\Delta x \Delta y$ and over the z-component for better visibility and the black lines represent the induction coil. These three timesteps and the corresponding coil fluxes are also marked in Figure 16d. As the (+) monopole approaches (1st. pos.), its fieldlines $\mathbf{B}_m = \frac{g}{r^2}\vec{e}_r$ cross the coil and the flux $\overline{\mathbf{B}}_m$ grows. Once it has passed the coil, $\mathbf{B}_{mon}$ crosses it from the other side, this direction change causes the change in sign $-\overline{\mathbf{B}}_m$. However if the dirac string is included $\overline{\mathbf{B}}_{m+dirac}$, no change of sign occurs and the flux continues smoothly increasing. Again, the dirac string is here given by the total field, $\overline{\mathbf{B}}$ is simply the sum over all spin values in the coil (considering direction).

While the right plot shows the fluxes over time as the monopole follows its trajectory, the left plot uses the orthogonal distance to the coil as the independent variable. This plot has been sketched in many publications but we were able to quantify it. The time-dependent plot is a good introduction to the monopole noise study.

We can generalize the ballistic, predefined trajectory to a set of configurations $\mathbf{M}^t$ drawn from a monte-carlo simulation according to grand-canonical or canonical ensembles that possibly includes generation and recombination of monopoles. With the previous formulas, this would result in a stochastic, physical induction curve $\overline{\mathbf{B}}_{total}^t$ that can be compared to experiments. Exactly that has been done by another research groups [15], however finding a signature flux distribution for monopoles has been proven difficult. We hope for the Helmholtz decomposition to shed light into the underlying processes.

[19] The path passes through the coil, preserves the total number of monopoles Q_{abs} to avoid GR noise. It is nevertheless not a straight path, this is the reason why we have two different plots, from which one can see that the trajectory is all but a straight line.

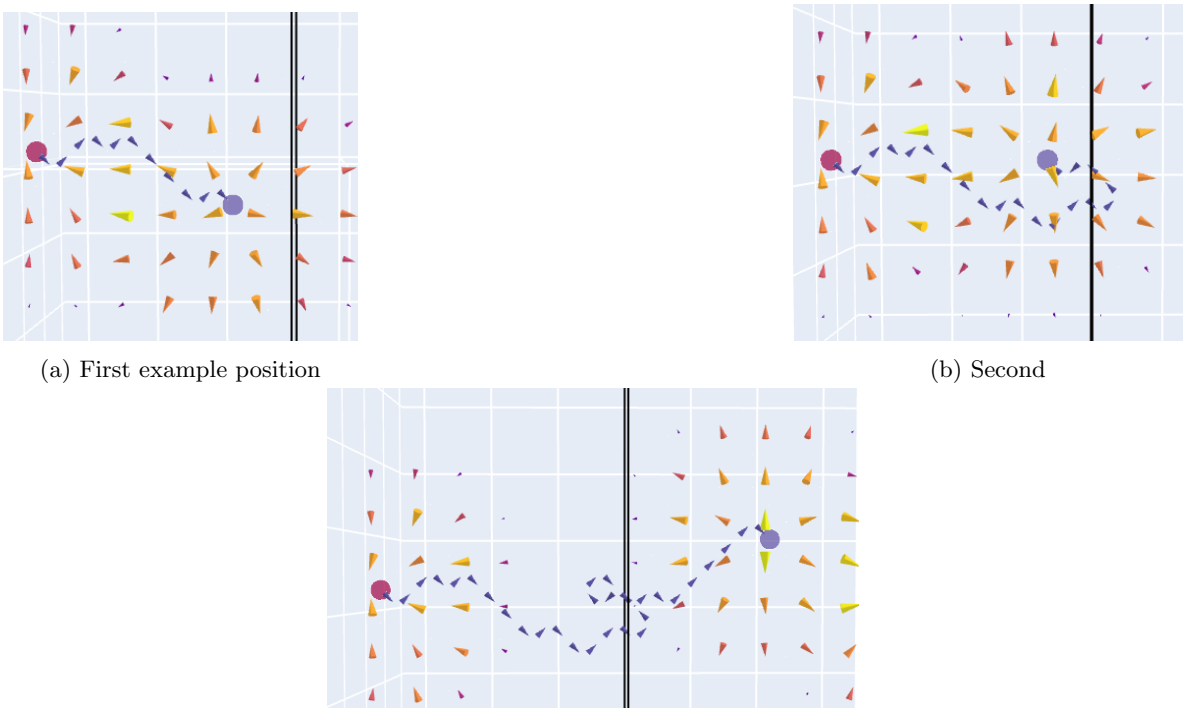

(a) First example position

(b) Second

(c) Third

Figure 12: The orange cones represent the (coarse grained) monopolar part of the field Φ_m. The blue spins are identified with the classical dirac string $\mathbf{M}_{dirac} = \mathbf{M}_f - \mathbf{M}_0$ along the path of monopole propagation. The dark lines represent the side view of the SQUID coil.

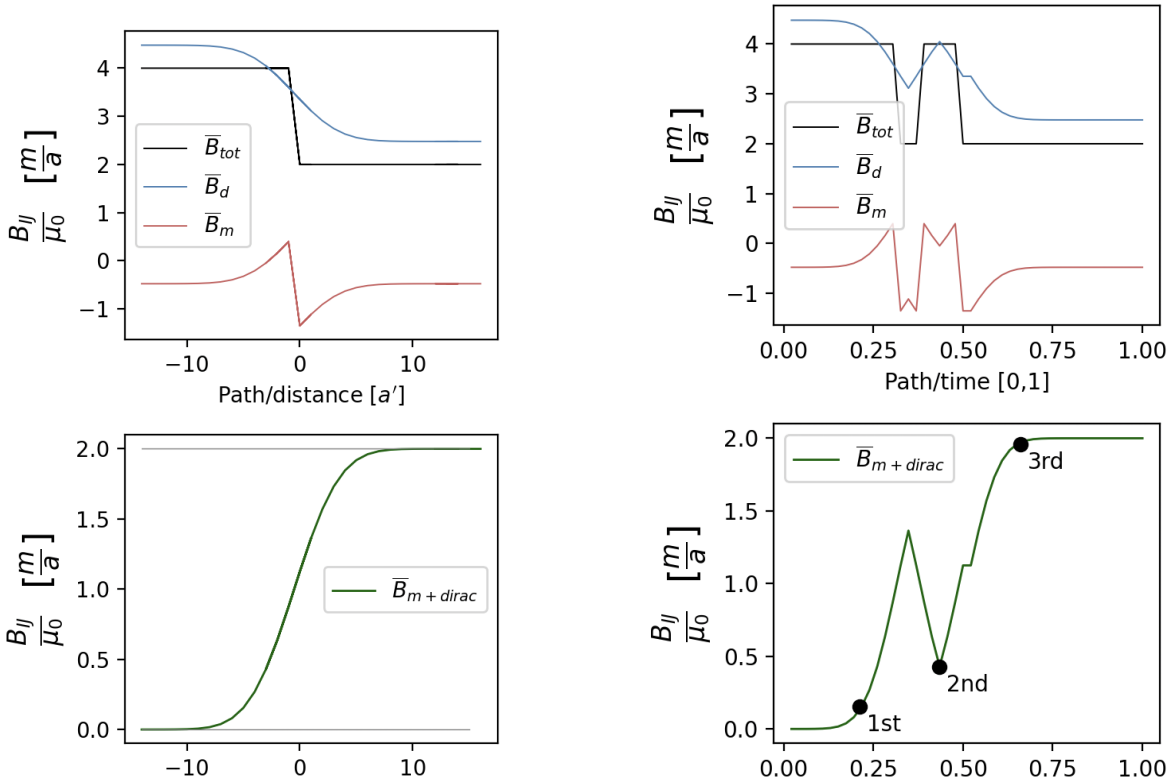

(a) Induction over the distance to the coil $\Delta y = y_{monop} - y_{coil}$.

(b) Induction over path time, counting each of the spin flips along the path.

Figure 13: Induction curves on the SQUID coil for the propagation of a +-monopole along the path. The left figure effectively folds the inductions of the right figure into a smooth induction curve.

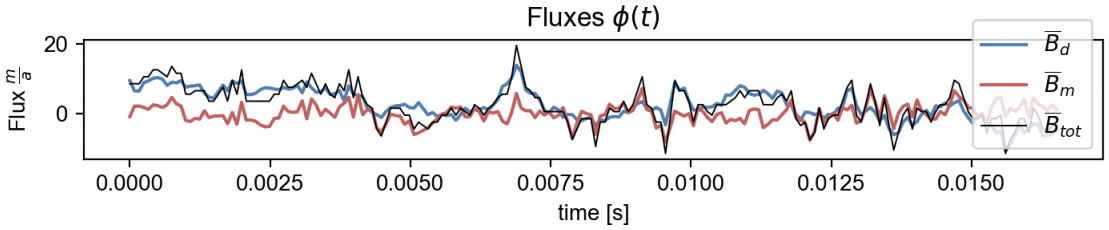

Figure 14: An example of the induction components for the thermalized system. In the following we will use 4 samples à 50K MC steps

5 Stochastic process of monopole noise

As it is well known, a classical ensemble of free, Coulomb interacting pointlike charges would be unstable, the stability being achieved by resorting to the quantum-mechanical behaviour of the electrons in atoms and the exclusion principle, although this topic is still being debated at present [14]. Luckily, the lattice character of our simulations evades problems such as potential tunneling and numerical instability due to diverging forces at small distances, replacing this with the recombination process, in which opposite $\pm g$ charges cancel each other out if they reach the same site. We can then safely focus on analyzing the signal induced by the Coulomb phase on the solenoid, but have to consider the constraints imposed by the pyrochlore lattice.

We make our take on the topic, arguing about typical correlation functions and their corresponding power spectra, we will try to connect them to the presented Langevin equations in eq. (17) and draw new conclusions about the diffusive dynamics of this process. We will first prove the validity of our simulations through comparison with [15] and enrich them with the Helmholtz decomposition to shed light on the dynamics of the topologically constrained Coulomb phase.

5.1 Generation of monte-carlo samples

For the next task, we generate four time $50K$ configurations $\mathbf{M}^t$ via Monte-Carlo simulation on a lattice of 4^3 unit cells, using a slightly modified C++ code from a former PhD student [11]. As in the ballistic example, we decompose each configuration $\mathbf{M}^t_{tot} = \mathbf{M}^t_d + \mathbf{M}^t_m$; the monopolar component $\mathbf{M}^t_m$ then contains a grand-canonical ensemble of the emergent Coulomb plasma[20], while the dipolar component $\mathbf{M}_d$ also includes the dirac string connecting monopole pairs, which will cause long-time correlations. We have seen that $\mathbf{M}_d$ has another interpretation: That it constitutes the additional, divergenceless degrees of freedom of the system. That will explain the different dynamics. Each component contributes to the (unphysical) induction as the sum over the spins that are inside the coil as in eq. (34):

$$\Phi^t_{tot,d,m} = \overline{\mathbf{B}}^t_{tot,d,m} \tag{38}$$

where

$$\boxed{\Phi^t \approx \overline{\mathbf{B}}^t_{m+dirac}} \tag{39}$$

is the physical induction of magnetic monopoles measured by the coil for a thermal sample; a new insight to preceding studies [15]. We proved (eq. 34) that this is the quantity that produces the induction $\int \mathbf{B} d\mathbf{S}$. Figure 14 is a display of the flux components measured by the coil in the thermalised sample with $T = 1K$.

[20] Constrained to the lattice

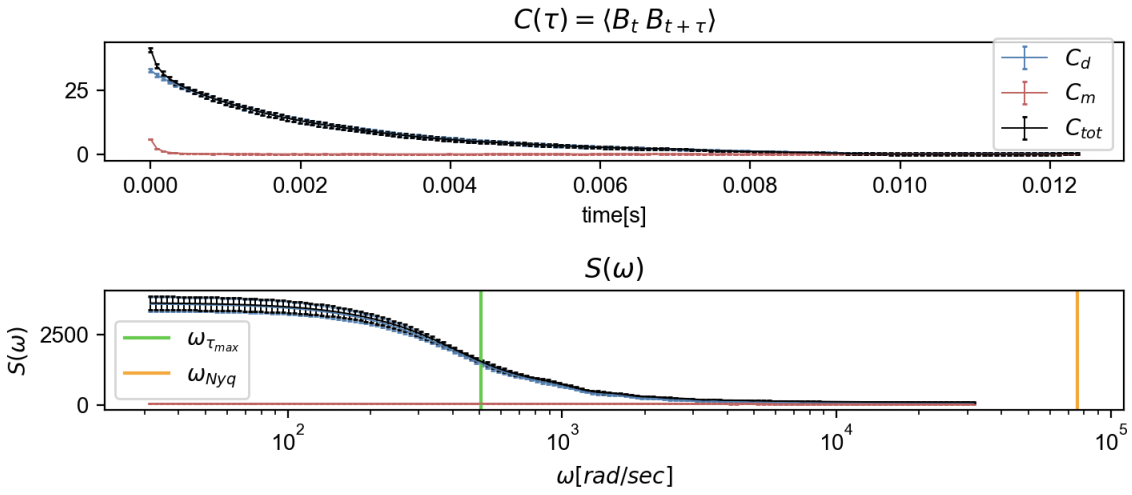

[h]

Figure 15: Computed correlation function in the chosen lag window $\tau \in [0, 0.012]$ for the m (red), d (blue) and their sum *tot* (black) and their power spectra. We can already identify that the m part decays way faster and has a far weaker signal.

5.2 Power spectra and Wiener-Chintschin-Theorem

This theorem lays down the definition of the power spectra of a stationary process as the cosine decomposition of the autocorrelation function[21]. Because the latter is a real and even function, the fourier-transform will also be real and even. We will consider two random variables, the monopole number N and the coil flux(es) Φ. In the example of the observable Φ, the autocorrelation function is

$$C_\Phi(\tau) = \langle \Phi(t) \cdot \Phi(t+\tau) \rangle_{eq} = \lim_{t_f \to \infty} \int_0^{t_f} \Phi(t)\Phi(t+\tau)dt \tag{40}$$

which we will not normalize to permit strong fluxes contribute more to the power spectra. We will compute the aucorrelation in a range $[\tau_{nyq}, \tau_{max}]$ constrained by the smallest possible *lag* given by the sampling or Nyquist time τ_{nyq} and the largest possible lag τ_{max} which still yields a good result given our limited simulation time t_f (see appendix B for a discussion on sampling effects). Then the power spectra is

$$S_\Phi(\omega)[C(\tau)] = \int_{-\infty}^{\infty} C(\tau) cos(\omega\tau) \tag{41}$$

5.3 Results for Monopole noise

One can fourier-transform the Langevin equation 17 [12] or simply use an exponential ansatz in $C(\tau)$ to obtain a first prediction for the power spectra of flux:

$$S(\omega)\,[C(\tau)] = S(\omega)\left[e^{-|\tau/\tau_0|}\right] \propto \frac{|\tau_0|}{1 + (\omega\tau_0)^b} \tag{42}$$

Following [15], we leave the exponent in the denominator free, but beware that to a decaying exponential corresponds $b = 2$[22]. We fitted this form into the simulated power spectras $S_{tot,d,m}(\omega)$ (Figure 15) and found following parameters for the different components:

[21] The same power spectra can be achieved by taking directly the squared modulus of the fourier transform, which we could sadly not confirm

[22] We could not find the analytical form of $C(\tau)$ if $b \neq 2$

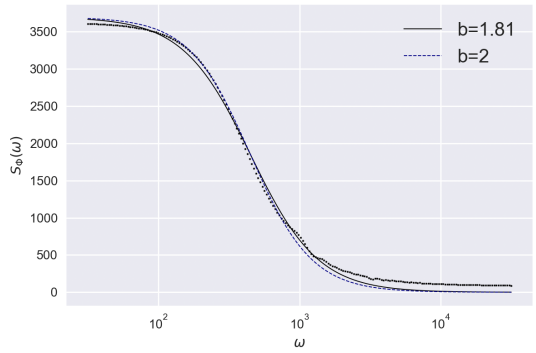

(a) Fit of the power spectra of Φ_{tot}.

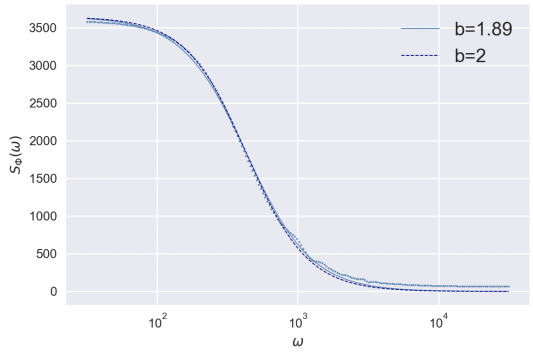

(b) Fit of the power spectra of Φ_d.

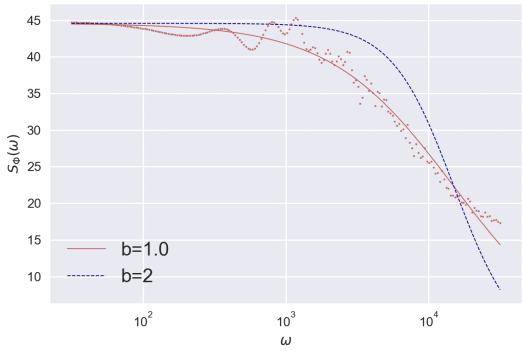

(c) Fit of the power spectra of Φ_m.

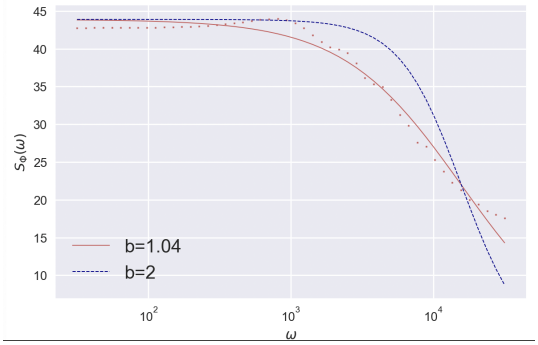

(d) A better suited τ range leave the fit parameters mainly unchanged.

Figure 16: Using the Ansatz of eq. 42, we fitted the different components and found the parameters, b being the slope after the plateau.

Component	Relaxation τ_0 $[ms]$	Exp b
Reference [15] (tot)	[0.5, 2.5]	[1.6, 2]
d	2 ± 0.02	1.89 ± 0.02
m	0.06 ± 0.003	0.99 ± 0.02
tot	2.2 ± 0.02	1.8 ± 0.02

Table 1: Found parameters after fitting the form of eq. 42, compared to the reference

in good agreement with the reference and the expected values for the topologically constrained Dipolar Spin Ice (DSI) model ($b_{DSI} = 2$) [15]. The fitted form as compared to the components of the simulated power spectra are displayed in Figures 16.

Some promising features were found in the analysis, like the $C_{tot}(\tau)$ kink at low τ (Figure 15) that seems to originate from the sum of two decaying exponentials with different timescales. The general relation between the correlation functions is not trivial but we have provided a relation in appendix D. The weak signal of m can be forwardly explained by the low density of monopoles at $T = 1K$, while the d component (with string), which leaves a lasting signal behind, has much larger amplitude. Also, the dirac string in d causes very long-time correlations to appear. We therefore identify two different decaying exponentials in $C_{m,d}(\tau)$, one for each component. Both characteristic decaying times can be found through the fit of $S_{m,d}(\omega)$ and are consistent with the reference. We notice however that by letting the parameter b free, we deviate from the exponential form, but could not find the analytic expression for $C(\tau)$. Nevertheless, we can safely assert that d decays much slower than m, and that the dirac string is the cause for such long-time correlation. Moreover, it is interesting that the m component yields $b \approx 1$, but we could not find an explanation.

A missing feature is that of characteristic frequencies, that could reflect the fact that the monopoles move in a highly constrained lattice, which we hypothesize should be the origin for oscillatory behaviour in the induction. This could have been the frequency description originally seeked, and also missed by [15]. The choice of the considered lag window $\tau \in [0, \tau_{max}]$ changes the behaviour of the power spectra

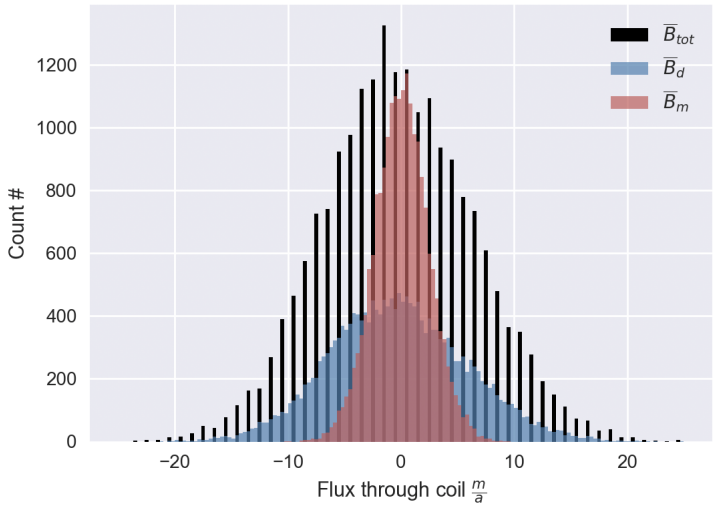

Figure 17: A histogram of the MC generated fluxes. While the sum of discrete spins must take discrete values, the decomposed values are continuous.

drastically, this does however also not yield any oscillatory behaviour.

We will lastly examine the histogram of the values recorded in figure 14, which we display in figure 17. We recall that the sum of the original spin fluxes[23] over the coil $\overline{\mathbf{B}}^t_{tot} = \mu \sum_{IJ}^{coil} \mathbf{M}^t$ must give multiples of $\frac{m}{a}$, as we can confirm. The decomposed parts take continuous values and all three colors in this plot cover equal areas, corresponding to the number of samples counted ($20K$). We can extract the variances and find $\sigma_d^2 = 33.38\frac{m}{a}$ and $\sigma_m^2 = 5.82\frac{m}{a}$ as well as the covariances from appendix D, $\sigma_d\sigma_m \approx 2.45\frac{m}{a}$, in good agreement with the correlation functions at $\tau = 0$: $C_d(0) = 32.88$, $C_m(0) = 5.75$. Higher moments are almost vanishing, pointing to a pure Gaussian, which probably implies that the sum has been performed over *Identical and independent random variables*. However the main point of the noise study was to find the correlations and their frequency dependence. This opens the question whether using N spin-flips on average for each monte carlo step was a good strategy, as it could have missed fast correlations of interest, possibly even the oscillatory behaviour.

6 Discussion

The Helmholtz decomposition has helped us separate monopolar and dipolar parts which play different roles in induction experiments. We found that the current felt by a solenoid placed around a spin-ice crystal actually measures $\Phi = \overline{\mathbf{B}}_{m+dirac}$, which can be also obtained from $\overline{\mathbf{B}}^t_d - \overline{\mathbf{B}}^0_d$. This made not a big difference in our *cold* ($T = 1K$), monopole-poor (≈ 20) experiments, where the monopolar component m was vanishingly small and we are in a regime where $\overline{\mathbf{B}} \approx \overline{\mathbf{B}_d}$. It remains open whether spin-ice at hotter temperatures manage to make a difference in our findings due to high monopole density. Highly fluctuating monopolar components and their induction $\overline{\mathbf{M}}_m$ could break the latter approximation and make a difference, entering a regime where the predictions from [15] would fail.

Furthermore we argue that the fits shown in Figure 16 show a systematic error but a analytic form corresponding to $b \neq 2$ could be found for $C(\tau)$. Perhaps further degrees of freedom can be added to better describe the monopole dynamics. Assuming a more general Ansatz as in equation 49 seems reasonable to us, considering the topological constraints in spin-ice. Having for example all spins but the last column pointing into the $+x$ direction[24], there remains no other option but to flip spins into $-x$, which necessarily translates into a decreasing induction current. We argue that at typical times, negative correlation values must appear to reflect this fact. The typical times would give a sort of *Resonance frequency* of the system. Disappointingly, the power spectra only shows the featureless form

[23] Which is the unit after having integraded over the area as in eq. 15. This also gets rid of the crossing angle dependence

[24] Meaning the last column is filled with sinks in $\mathbf{M}$

shown in this report.

Moreover we argue that the problematic generation-recombination (GR) ratio deeply discussed in [15] is very easy to get rid of by prohibiting monopole number fluctuations in the monte carlo simulation. This modification will be the next step towards monopole noise analysis.

Another interesting comparison of the noise would be that for a free plasma of electrically or magnetically charges in periodic boundary conditions, and the induced current on a superconductive solenoid. Comparison with our study should yield the differences coming from the topological constraints of spin ice, and could help in identify a more general monopole noise signature. Lastly, the 't Hooft–Polyakov monopoles [2][3] were derived by succesfully avoiding both singularities in $\mathbf{A}$ and the Dirac string. It is possible that this monopoles also have condensed matter analogues and this possibility should be studied.

A Singularities in gauge theory

Assuming we want to develop a theory for magnetic monopoles which are a source of magnetic field only: $\nabla \cdot \mathbf{B} = \rho_{magn} \neq 0$. For example for a monopole at the origin:

$$\mathbf{B}_{mon} = \frac{g}{r^2}\vec{e}_r \tag{43}$$

we will review physical laws that stand in contradiction to it, and explain Dirac's motivation to introduce the strings.

A.1 Classical electromagnetism

Maxwell conceived electromagnetism without magnetic monopoles $\nabla \cdot \mathbf{B} = 0$ so that the physical fields $\mathbf{E}$ and $\mathbf{B}$ could be described in terms of the electric scalar potential φ and magnetic vector potential $\mathbf{A}$ through:

$$\mathbf{E} = -\nabla\varphi - \frac{\partial \mathbf{A}}{\partial t} \qquad \mathbf{B} = \nabla \times \mathbf{A} \tag{44}$$

Hereby $\mathbf{E}$ and $\mathbf{B}$ remain invariant under the simultaneous gauge transformations:

$$\mathbf{A} \mapsto \mathbf{A} + \nabla\Psi \tag{45}$$

$$\varphi \mapsto \varphi - \frac{\partial \Psi}{\partial t} \tag{46}$$

for any arbitrary gauge function $\Psi(\mathbf{x}, t)$ [25]. This formulation, which has proven indiscutable, already prevented monopoles because the well-known definition $= \nabla \times \mathbf{A}$ implies $\nabla \cdot (\nabla \times \mathbf{A}) = 0$. However since at the time φ and $\mathbf{A}$ were mere mathematical conveniences, this wasn't a fatal blow for magnetic monopoles - maybe classical electromagnetism could just be reformulated.

A.2 Coupling of quantum-mechanics with classical electromagnetism

With the advent of quantum mechanics, it became clear that the wavefunction of an electrically charged particle coupled directly to $\mathbf{A}$. This was accurately predicted and experimentally verified for the Aharonov–Bohm effect (see section 1.2). It became clear that $\mathbf{A}$ was itself physical, so its divergenceless property could not be avoided anymore:

$$\nabla \cdot (\nabla \times \mathbf{A}) = 0 \tag{47}$$

Trying to describe $\mathbf{B}_{mon}$ through a universal vector potential $\mathbf{A}_{mon}$ led to a necessary singularity (undefined value) of $\mathbf{A}_{mon}$ at the origin of the source, where $\nabla \cdot \mathbf{B}_{mon} = 4\pi g\delta(x)$. The solution Dirac envisioned introduced a string carrying flux away from the sink and into the source monopole[26]:

$$\mathbf{B}_{ms} = \mathbf{B}_{mon} + 4\pi g\delta(x)\delta(y)\Theta(-z)\vec{e}_z \tag{48}$$

ensuring $\nabla \cdot \mathbf{B}_{ms} = 0$ everywhere and permitting the description through a global $\mathbf{A}$, making the idea of magnetic monopoles [27] consistent with classical and quantum physics. Imposing unobservability of this string leads to Dirac's quantization condition.

B Low sampling effects

We expect the correlation function $C(\tau)$ at large lags τ to be increasingly difficult to determine from the MC samples $\Phi(t)$ due to the continuously worsening signal to noise ratio as $\tau \to \infty$. This is

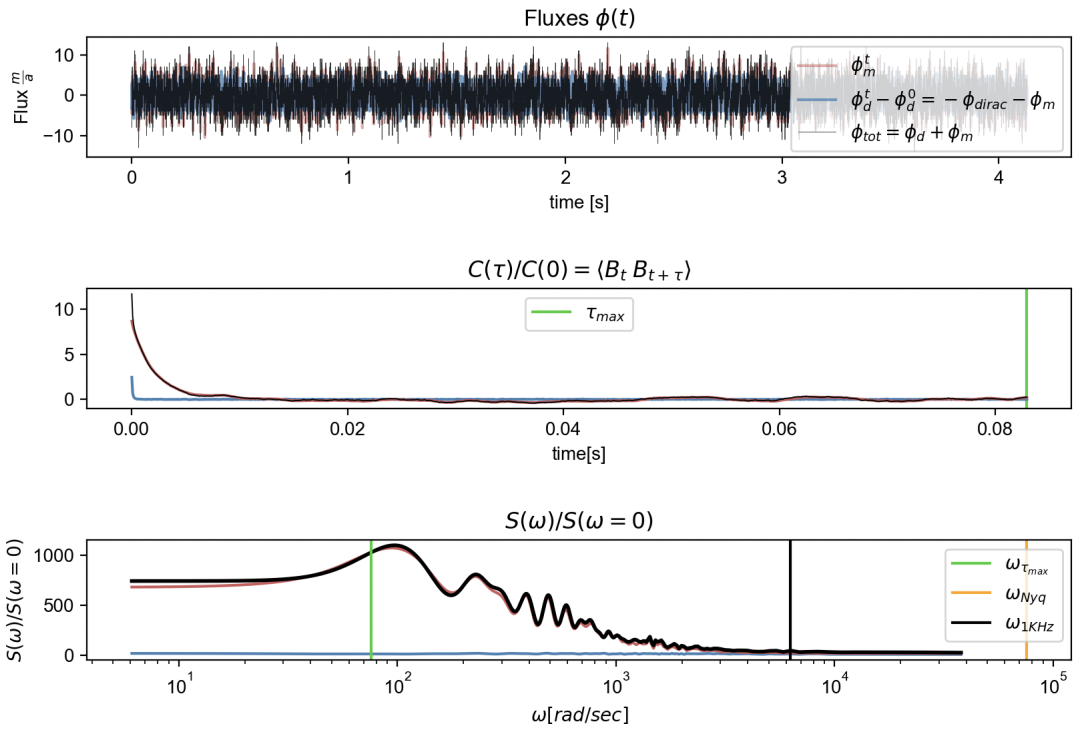

Figure 18: Considering too large τ values results in a correlation function that has not sufficiently averaged out the noise. This error projects onto the power spectra, giving peaks at random frequencies.

inherent to random processes as values of $\Phi(t+\tau)$ become more and more difficult to predict from a previous $\Phi(t)$. Here is a bad example where the considered window in τ was chosen too long.

We have to tackle down this problem either by sampling more MC steps or by reducing the considered τ window in question.

C Possible oscillatory modes of monopole noise

While growing our dataset, it is still not clear whether the correlation functions actually go into the negative regime, which would point out to an oscillatory behaviour of the flux Φ_t itself[28]. This option is still open and rich, as it must be defined via characteristic frequencies. A typical correlation function containing characteristic frequencies could have the form:

$$C(\tau) = e^{-\tau/\tau_{rel}} \cdot \cos\left(\omega_C \cdot \tau - \tau_0\right) \tag{49}$$

with power spectra:

$$S_\Phi(\omega) = \int C(\tau) \cdot \cos\omega(\tau) d\tau \tag{50}$$

This has been already modelled for dipole moment in dilute gases or the displacement of a harmonic oscillator in a bath [17]. The actual behaviour in this work is until now assumed to have a relaxational form, as can be seen from the assumed form of the Langevin equation:

[25]This corresponds to the $U(1)$ gauge freedom of electromagnetism.
[26]Positioned in the infinite
[27]Which truly are just extended dipoles with $\nabla \cdot \mathbf{B} = 0$
[28]A positive deviation is statistically going to lead to a negative deviation after a time τ, and conversely. This is often encoded into the Langevin equation via an Inertia/Negative memory/negative friction term that causes the oscillations

$$m\frac{dv}{dt} = -\lambda v + \eta(t) \tag{51}$$

whose correlation function is just a decaying exponential with relaxation $\tau = \frac{m}{\lambda}$.

D Relation between correlation function components

From the definition of a correlation function and the decomposition of the induction into its components:

$$C_{tot}(\tau) = \langle \overline{\mathbf{B}}^t \overline{\mathbf{B}}^{t+\tau} \rangle_t^{eq} = \langle (\overline{\mathbf{B}}_m^t + \overline{\mathbf{B}}_d^t)(\overline{\mathbf{B}}_m^{t+\tau} + \overline{\mathbf{B}}_d^{t+\tau}) \rangle = \langle \overline{\mathbf{B}}_m^t \overline{\mathbf{B}}_m^{t+\tau} \rangle + \langle \overline{\mathbf{B}}_m^t \overline{\mathbf{B}}_d^{t+\tau} \rangle + \langle \overline{\mathbf{B}}_d^t \overline{\mathbf{B}}_m^{t+\tau} \rangle + \langle \overline{\mathbf{B}}_d^t \overline{\mathbf{B}}_d^{t+\tau} \rangle \tag{52}$$

the second term can be rewritten as the third, using the fact that the random variables are in a steady state and have time-shift symmetry and time-reversal symmetry:

$$\langle \overline{\mathbf{B}}_m^t \overline{\mathbf{B}}_d^{t+\tau} \rangle \overset{ss}{=} \langle \overline{\mathbf{B}}_m^{t-\tau} \overline{\mathbf{B}}_d^t \rangle \overset{\tau=-\tau}{=} \langle \overline{\mathbf{B}}_d^t \overline{\mathbf{B}}_m^{t+\tau} \rangle \tag{53}$$

so that we can simplify:

$$C_{tot}(\tau) = C_m(\tau) + 2 \cdot \langle \overline{\mathbf{B}}_d^t \overline{\mathbf{B}}_m^{t+\tau} \rangle + C_d(\tau) \tag{54}$$

and computation of the second term gives the covariance (Figure 19) of the components for a given lag τ. The cross term contribution at zero lag is therefore ≈ 2.45 as compared with the variances $\sigma_d^2 = 33.38\frac{m}{a}$ and $\sigma_m^2 = 5.82\frac{m}{a}$ (section 5.3) and can't be ignored. The relaxation timescale is in the order of $10^{-4}[s]$ showing extremely fast decorrelation. We also have another hint for the oscillatory behaviour of the obversables.

Figure 19: Covariance of the different components is half the cross term in $C_{tot}(\tau)$

References

[1] P. Dirac, "Quantised singularities in the electromagnetic field," *Proc. R. Soc. Lond. A*, pp. 60–72, 1931.

[2] G. 't Hooft, "Magnetic monopoles in unified gauge theories," *Nuclear Physics B*, vol. 79, no. 2, pp. 276–284, Sep. 1974. DOI: 10.1016/0550-3213(74)90486-6.

[3] A. M. Polyakov, "Particle spectrum in the quantum field theory," Tech. Rep., 1974. [Online]. Available: https://cds.cern.ch/record/417863.

[4] B. Cabrera, "First results from a superconductive detector for moving magnetic monopoles," *Phys. Rev. Lett.*, vol. 48, pp. 1378–1381, 20 May 1982. DOI: 10.1103/PhysRevLett.48.1378. [Online]. Available: https://link.aps.org/doi/10.1103/PhysRevLett.48.1378.

[5] S. T. Bramwell and M. J. P. Gingras, "Spin ice state in frustrated magnetic pyrochlore materials," *Science*, vol. 294, no. 5546, pp. 1495–1501, Nov. 2001, ISSN: 1095-9203. DOI: 10.1126/science.1064761. [Online]. Available: http://dx.doi.org/10.1126/science.1064761.

[6] R. Burgess, "The statistics of charge carrier fluctuations in semiconductors," *Proceedings of the Physical Society. Section B*, vol. 69, p. 1020, Dec. 2002. DOI: 10.1088/0370-1301/69/10/308.

[7] C. Castelnovo, R. Moessner, and S. L. Sondhi, "Magnetic monopoles in spin ice," *Nature*, vol. 451, no. 7174, pp. 42–45, Jan. 2008, ISSN: 1476-4687. DOI: 10.1038/nature06433. [Online]. Available: http://dx.doi.org/10.1038/nature06433.

[8] L. D. C. Jaubert and P. C. W. Holdsworth, "Signature of magnetic monopole and dirac string dynamics in spin ice," *Nature Physics*, vol. 5, no. 4, pp. 258–261, Mar. 2009, ISSN: 1745-2481. DOI: 10.1038/nphys1227. [Online]. Available: http://dx.doi.org/10.1038/nphys1227.

[9] L. D. C. Jaubert and P. C. W. Holdsworth, "Magnetic monopole dynamics in spin ice," *Journal of Physics: Condensed Matter*, vol. 23, no. 16, p. 164 222, Apr. 2011, ISSN: 1361-648X. DOI: 10.1088/0953-8984/23/16/164222. [Online]. Available: http://dx.doi.org/10.1088/0953-8984/23/16/164222.

[10] M. E. Brooks-Bartlett, S. T. Banks, L. D. C. Jaubert, A. Harman-Clarke, and P. C. W. Holdsworth, "Magnetic-moment fragmentation and monopole crystallization," *Phys. Rev. X*, vol. 4, p. 011 007, 1 Jan. 2014. DOI: 10.1103/PhysRevX.4.011007. [Online]. Available: https://link.aps.org/doi/10.1103/PhysRevX.4.011007.

[11] V. Kaiser, "The wien effect in electric and magnetic coulomb systems - from electrolytes to spin ice," Oct. 2014.

[12] A. V. Klyuev, M. I. Ryzhkin, and A. V. Yakimov, "Statistics of fluctuations of magnetic monopole concentration in spin ice," *The Random and Fluctuating World*, 2017. [Online]. Available: https://api.semanticscholar.org/CorpusID:126295052.

[13] R. Heras, "Dirac quantisation condition: A comprehensive review," *Contemporary Physics*, vol. 59, no. 4, pp. 331–355, Oct. 2018, ISSN: 1366-5812. DOI: 10.1080/00107514.2018.1527974. [Online]. Available: http://dx.doi.org/10.1080/00107514.2018.1527974.

[14] M. Apostol and L. Cune, "On the stability of a classical plasma," *Physics Letters A*, vol. 383, no. 16, pp. 1831–1835, 2019, ISSN: 0375-9601. DOI: https://doi.org/10.1016/j.physleta.2019.03.018. [Online]. Available: https://www.sciencedirect.com/science/article/pii/S0375960119302464.

[15] R. Dusad, F. K. K. Kirschner, J. C. Hoke, *et al.*, "Magnetic monopole noise," *Nature*, vol. 571, no. 7764, pp. 234–239, Jul. 2019, ISSN: 1476-4687. DOI: 10.1038/s41586-019-1358-1. [Online]. Available: http://dx.doi.org/10.1038/s41586-019-1358-1.

[16] D. Slobinsky, L. Pili, and R. A. Borzi, "Polarized monopole liquid: A coulomb phase in a fluid of magnetic charges," *Phys. Rev. B*, vol. 100, p. 020 405, 2 Jul. 2019. DOI: 10.1103/PhysRevB.100.020405. [Online]. Available: https://link.aps.org/doi/10.1103/PhysRevB.100.020405.

[17] A. Tokmakoff, "Time-correlation functions," *Chem Libretext*, 2019. [Online]. Available: http://home.uchicago.edu/~tokmakoff/TDQMS/Notes/5.%20Time-Corr%20Funcs%203-08.pdf.

[18] A. H. Zapke, "Signature of quasi magnetic monopoles in spin-ice, fragmented gauge fields in real and reciprocal space," 2023.